



# Dispersion mechanism-induced variations in microstructural and mechanical behavior of CNT-reinforced aluminum nanocomposites

Kemal Doğan<sup>1</sup> · Muhammed İhsan Özgün<sup>2</sup> · Halit Sübüta<sup>3</sup> · Emin Salur<sup>3</sup> · Yasin Eker<sup>2</sup> · Mustafa Kuntoğlu<sup>4</sup> · Abdullah Aslan<sup>5</sup> · Munish Kumar Gupta<sup>6</sup> · Mustafa Acarer<sup>3</sup>

Received: 24 August 2021 / Revised: 12 December 2021 / Accepted: 1 January 2022 / Published online: 24 January 2022  
© The Author(s) 2022

## Abstract

The combination of powder metallurgy and ball milling method has been widely regarded as the most beneficial route for producing multi-walled carbon nanotubes (MWCNTs)-reinforced aluminum matrix composites. In this study, the effects of different milling times (1, 2, 4, and 8 h) on the structural, morphological, and crystallographic properties of MWCNTs-reinforced Al7075 composite powders were characterized by particle size analyzer, Raman spectroscopy, scanning electron microscopy (SEM), high-resolution transmission electron microscopy (HR-TEM), and X-ray diffraction (XRD). After the morphological and structural characterization of the milled powders, the microstructural and mechanical properties of the hot-pressed composites were evaluated using an optical microscope, SEM, density, and Brinell hardness measurements. Considering milled powder characterization, the MWCNTs were gradually distributed and embedded within the matrix as the milling time increased. Milling for 8 h resulted in a minimum level of particle size (11 µm) with shortened and uniformly dispersed CNTs. Brinell hardness of the composite increased from 91 to 237 HB -a ~%160 after 8 h of milling. Such a remarkable increment in hardness could be attributed to several concurrent strengthening effects related to dispersion, solution, grain refinement, and Orowan looping mechanisms. However, relative density results revealed that the composite produced by 2 h milled powders exhibited the highest density (%99.96). The observed differences between hardness and density results were ascribed to powders' deteriorated packing and sintering behavior due to an increment in the hardness of particles and variation in particle size range and morphology, which resulted from following different milling protocols.

**Keywords** Aluminum · Carbon nanotubes · Ball milling · Hot pressing · Microstructural characterization

✉ Munish Kumar Gupta  
munishguptanit@gmail.com

Kemal Doğan  
kmlgdgn63@gmail.com

Muhammed İhsan Özgün  
miozgun@erbakan.edu.tr

Halit Sübüta<sup>3</sup>  
halit.subutay@selcuk.edu.tr

Emin Salur  
esalur@selcuk.edu.tr

Yasin Eker  
yeker@erbakan.edu.tr

Mustafa Kuntoğlu  
mkuntoglu@selcuk.edu.tr

Abdullah Aslan  
aaslan@selcuk.edu.tr

Mustafa Acarer  
macarer@selcuk.edu.tr

<sup>1</sup> Department of Nanotechnology and Advanced Materials, Institute of Science, Selcuk University, 42075 Konya, Turkey

<sup>2</sup> Metallurgical and Material Engineering Department, Necmettin Erbakan University, 42090 Konya, Turkey

<sup>3</sup> Metallurgical and Material Engineering Department, Technology Faculty, Selcuk University, 42075 Konya, Turkey

<sup>4</sup> Mechanical Engineering Department, Technology Faculty, Selcuk University, 42075 Konya, Turkey

<sup>5</sup> Department of Mechanical Engineering, Faculty of Engineering, Selcuk University, Akşehir, 42550 Konya, Turkey

<sup>6</sup> Faculty of Mechanical Engineering, Opole University of Technology, 76 Proszkowska St., 45-758 Opole, Poland

## 1 Introduction

Metal matrix composites (MMCs) have emerged due to the ineffectuality of traditional monolithic metals and their alloys in achieving a combination of various crucial features that are prerequisites in today's production technologies [1]. Among various MMCs, Al-based metal matrix composites (AMCs) have received more attention than conventional metal-based alloys thanks to their high specific mechanical properties, good machinability characteristics, lightweight, economical, and effortless accessibility. The most commonly used matrix material among Al alloys is the 7XXX series, which can be heat treated and exhibit higher mechanical properties than other aluminum alloys thanks to their minor alloying elements (Zn, Mg, Cu) [2]. Recently, aluminum metal matrix nanocomposites (AMNCs), which are reinforced with different nano-reinforcement materials (oxide, carbide, nitride), have fascinated many researchers due to their superior overall properties as compared to the AMCs [3]. These properties have stemmed from the grain refinement mechanism provided by homogeneously distributed nano-sized reinforcements into the matrix.

The outstanding mechanical properties, high aspect ratio, unique atomic structure, low density, excellent chemical stability, and superior thermal and electrical properties of CNTs make them the most suitable reinforcement material for metal [4] and polymer [5] matrix composites. To meet the accelerating demands of lightweight, high specific mechanical properties, high corrosion resistance, good machining performance, and easy accessibility in material features for maritime, aerospace, and automobile industries, numerous researches have been carried out to explore new Al-based metal matrix nanocomposites [6]. However, CNT/Al systems still encounter some challenges due to the lower wettability and non-uniform distribution of CNTs within the Al matrix [7]. Therefore, different problems can be faced during the production of these composites by conventional methods such as casting and melting. Also, the formation of undesirable reactions depending on the elevating process temperature in liquid production methods such as stir casting, infiltration, and spray deposition adversely affects the mechanical properties [8]. Providing good interfacial bonding between the matrix and the reinforcement element is another main issue, directly or indirectly affecting the performance, fabrication, and application areas of materials [9].

Various processes such as metal injection molding [10], casting process [11], in situ synthesis [12], spray forming [13], physical and chemical vapor deposition [14], and powder metallurgy [15] have been used to produce CNT/Al nanocomposites. Among these techniques,

powder metallurgy (PM) is one of the most preferred processes in producing Al-based metal matrix nanocomposites (AMNCs). Although there are various PM methods to consolidate powders, mechanical alloying (MA) can eliminate segregation and aggregation of reinforcement elements within the matrix and supply fine dispersion of reinforcement particles into aluminum or different base metal systems with the volume fraction [16]. Apart from the MA method, various production methods, such as blending [4], stir casting [17], acidification [18], organic polymer process [19], arc melting [20], and subsequent heat treatments [21], have been employed to disperse the nanoparticles into the matrix. However, the techniques mentioned above have improved the mechanical properties of AMNCs to a limited extent, since most of the nanoparticles segregate and aggregate at the grain boundaries and cause poor interfacial bonding (wetting) between the reinforcement and matrix phase. The best sample for better structural integrity consists of a fine powder, supersaturated microstructure, or a dense homogenous distribution of fine reinforcement particles [22]. In our previous study [2], such microstructures for TiC-reinforced AMNCs was achieved by a fruitful combination of mechanical alloying and powder metallurgy routes.

Recently, MA has been widely applied to disperse the different types of carbide (TiC [2], B<sub>4</sub>C [23], SiC [24]), oxide (Al<sub>2</sub>O<sub>3</sub> [25], Y<sub>2</sub>O<sub>3</sub> [26]), and carbon-based (CNT [27], SWCNT [28], FWCNT [29], MWCNT [30]) reinforcements into Al-based composites. As a simple mechanical milling system, MA provides uniform nanocrystalline materials and nanocomposites due to excessive plastic deformation and fracture mechanism under the impact of tiny and rigid balls [15]. MA also effectually breaks the flexible tangled CNTs and leads to homogenous dispersion of the CNTs within the matrix [31]. Nevertheless, the structural and morphological evolution of CNTs is hardly controllable in the MA process due to many ball-milling parameters required to be optimized [32]. Esawi et al. [33] examined the effect of the reinforcement ratio of CNTs and their morphological structure on the mechanical properties of AMCs produced by mechanical alloying. They reported that the larger CNTs were distributed easier than smaller ones, which have a more substantial agglomeration potential. The composites' hardness and tensile properties improved profoundly with increased CNT content up to 2 wt.% and then worsened as the CNT content increased. Li et al. [34] produced Al matrix composites with different CNT content (1 and 2 wt.%) utilizing flake powder technology and hot extrusion process. They reported that enhanced strength and high elongation values were achieved in both composites, especially that the elongation value of the composite containing 2% CNT was 30% higher than that of pure aluminum fabricated with the same production history. They attributed this observed increase in mechanical properties to the strong interfacial

bonding between the shortened and homogeneously dispersed CNTs and the matrix, the fine and nearly equal grains formed during hot extrusion, and the formation of bridge-linked CNTs along the extrusion direction. As a function of milling time, Ostovan et al. [35] investigated the nanomechanical behavior of CNTs-reinforced Al matrix composites utilizing nanoindentation. They reported that the dispersion uniformity of CNTs within the matrix was highly influential on nanocomposites' mechanical properties. As the milling time increased, the elastic modulus and hardness of nanocomposites improved. However, they obtained lower hardness and Young's modulus in the early stage of milling due to the accumulation of CNTs at the grain boundaries.

As mentioned above, while various aspects of mechanical alloying in the context of Al alloys research were studied in great detail, the milling time seems to have received cursory attention, which is why we focus on it in this study to assess its ramification to great depth. No comprehensive information has been achieved about the effect of milling time on the dispersion behavior of CNTs, powder morphology, and crystallographic structure of milled CNTs/Al7075 nanocomposites, and their correlation between packing densities, consolidation behaviors, and resultant mechanical properties of produced MMCs have not been discussed. In this study, 1 wt.% CNTs-reinforced Al7075 matrix nanocomposites were successfully produced via a high-energy planetary ball milling followed by hot pressing. We carried out a comprehensive study about the effect of milling time on the powder morphologies and dispersion and damage of CNTs based on SEM, particle size and distribution, XRD (crystallite size, lattice strain, and dislocation density), Raman spectrometry, HR-TEM, and energy-dispersive spectroscopy. Furthermore, microstructures and mechanical properties of the hot-pressed CNTs/Al7075 nanocomposites were evaluated using optical microscopy, hardness, and relative density results.

## 2 Materials and methods

### 2.1 Powder characterization

As-received Al7075 powders (99.9% purity, < 43 μm particle size) and CNTs (about 5–10 nm in diameter and 5 μm in length) were purchased from Nanografi Nanotechnology, Co. Ltd., Ankara, Turkey, and employed in this study. The chemical composition of the Al7075 alloy powder is given in Table 1. Figure 1 shows the morphologies of the initial materials. To achieve a uniform dispersion of CNT with lower damage, the Al matrix was reinforced with 1 wt.% CNT. A

comprehensive literature search revealed that the CNTs content is preferred mainly between 0.2 and 2 wt.% for aluminum and other different base metal systems. It was observed that the addition of 1 wt.% CNT in the Al matrix significantly improved the mechanical properties, as reported by Deng et al. [36]. Kurita et al. [37] reported that the tensile strength and elongation to failure reached a maximum value when the CNT content was 1 wt.%. In this context, CNT content and other process parameters were determined by our preliminary tests, prejudice knowledge, and literature survey. As-received Al7075 and CNT powders were mechanically alloyed (MA) with tungsten carbide (WC) balls in a tungsten carbide jar utilizing RETSCH-PM 200 planetary ball milling device at a rotation rate of 450 rpm. The ball-to-powder (BPR) mass ratio was selected as 5:1, and the ball milling time was chosen as 1, 2, 4, and 8 h, respectively. To avoid cold working and clusters of the powders during milling, 1 wt.% concentration methanol was used as a process control agent (PCA). To prevent excessive temperature during milling, the powders were milled for 20 min, then rested for 10 min, and then milled again, etc., until the desired milling protocol was completed.

The morphologies of unmilled (as-received Al7075) and milled powders (CNTs/Al7075) were examined utilizing a field-emission scanning electron microscopy (SEM, Zeiss EVO LS10) and a high-resolution transmission electron microscopy (HRTEM, JEOL JEM-2100). Elemental analysis of the milled powders was determined by energy-dispersive X-ray spectroscopy (EDS). Besides, the average particle sizes (APS) and particle size distribution (PSD) of the powders were analyzed by particle size analyzer (Cilas 1190), using laser light diffraction. The damage and dispersion behavior of the CNTs were monitored by Raman spectroscopy (Renishaw, inVia™ confocal Raman microscope). An X-ray diffractometer (Malvern PANalytical, X'Pert<sup>3</sup> Powder) was employed to identify phase components, indexation of peaks of the milled powders. XRD data were collected with Cu-Kα radiation at a wavelength (λ) of 0.15406 nm by using a step-scan procedure with 0.1 degrees 2-theta per step and 10 s per step dwell time.

The crystallographic properties, namely average crystallite size, lattice strain, and dislocation density of the milled powders, were assessed by XRD data in conjunction with the Williamson–Hall [38] and Williamson–Smallman [39] equations as follows:

$$\beta_{hkl} \times \cos \theta = \left(0.9 \times \frac{\lambda}{D}\right) + (4 \times \epsilon \times \sin \theta), \quad (1)$$

**Table 1** Chemical composition of as-received Al7075 alloy powders

Element's concentration	Zn	Mg	Cu	Fe	Si	Al
(wt. %)	5.95	2.78	1.65	0.12	0.14	Balance

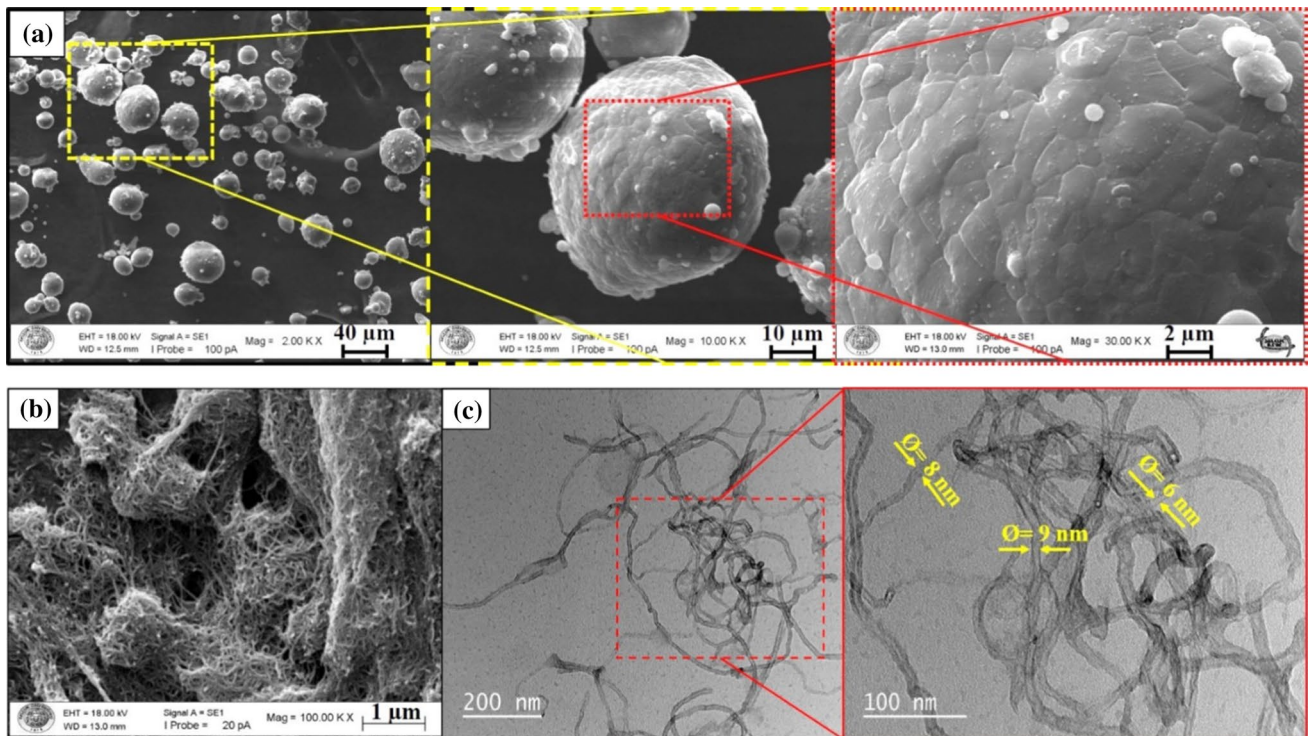


**Fig. 1** **a** SEM image of the as-received Al7075 powders, **b** SEM, and **(c)** HR-TEM images of the as-received multi-walled CNTs

$$\delta = n/D^2, \quad (2)$$

where  $\beta_{hkl}$  is the total broadening that was achieved by subtracting the instrumental broadening from the observed peak broadening,  $D$  is the crystallite size (coherently diffracting domain size), which is determined from full-width at half maximum (FWHM) of peaks,  $\varepsilon$  is the lattice strain (microstrain),  $\theta$  is the Bragg reflection angle, and  $\lambda$  is the wavelength of Cu-K $\alpha$  radiation. The dislocation density ( $\delta$ ), defined as the number of dislocation lines per unit volume in the crystalline material, was calculated by Eq. 2, where  $n \sim 1$  and  $D$  is the crystallite size [40].

## 2.2 Production process and composite characterization

After the powder characterization, the milled powders were compacted with the help of a hot pressing process, performed under 300 MPa and 435 °C for 1 h. Firstly, the milled powders were molded into the female die. Then, the powders were held at a constant temperature (435 °C) for 1 h in the female die for homogeneous temperature distribution. After the heating process, the compaction of the powders was achieved by the male dies' synchronic movement, and the MMCs were taken from the female die. The cylindrical samples with a length of 10 mm and a diameter of 10 mm were prepared. For comparison purposes, the as-received

Al7075 (unmilled/reference) specimen was also consolidated with the same producing history. However, the Raman spectrum was excluded for as-received Al7075 powders characterization since it is not suitable for the analysis of pure metals and their alloys [41]. The schematic view of ball milling process and production stage is illustrated in Fig. 2. The Brinell hardness values of composites were measured with a “Digirock-Lc-Rbov” tester under 62.5 kg load using 2.5 mm diameter indenter ball. The theoretical density of the composites was assessed by rule of mixtures, and its experimental density was measured with the “Precisa XB 220A” precise scale, utilizing the Archimedes principle [2]. The microstructural evolution of the composites was analyzed using optical microscopy (OM, Nikon Eclipse MA100 N) instrument.

## 3 Results and discussion

### 3.1 Effect of milling time on particle characteristics

Figure 3 shows the morphologies of the milled powders as a function of milling time. The average particle size (APS) of the 1 h milled powders was calculated as  $\sim 30 \mu\text{m}$  (as described in Fig. 4), the morphology of which is shown in Fig. 3a. After 1 h of milling, the particle shape of some powders changed to less spherical pieces (angular morphology),



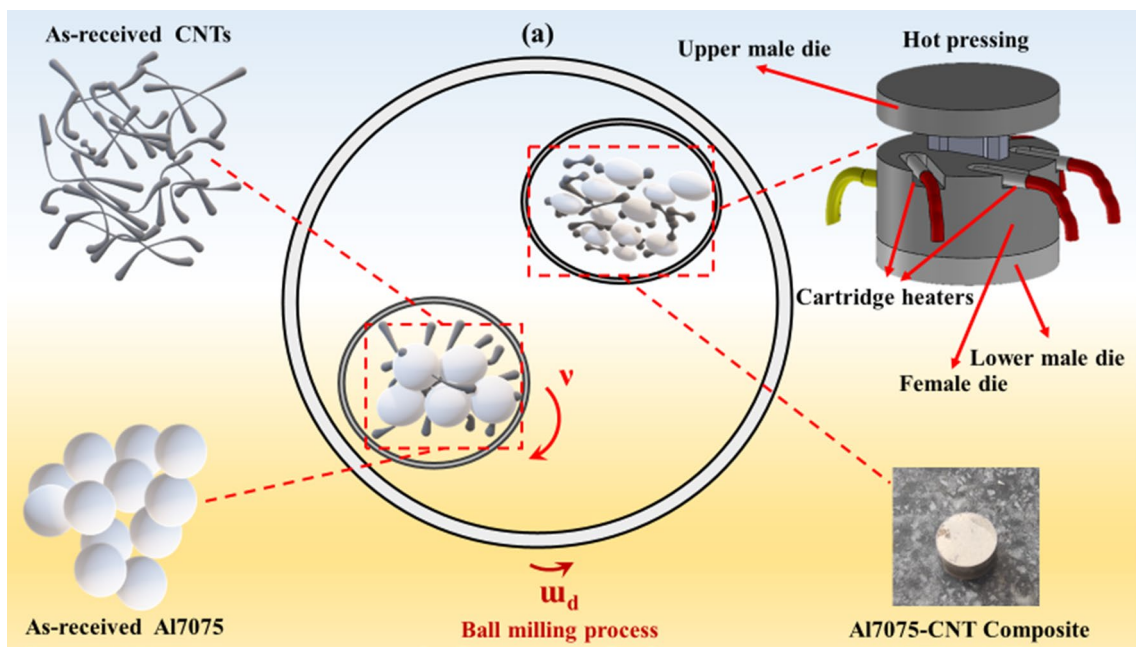
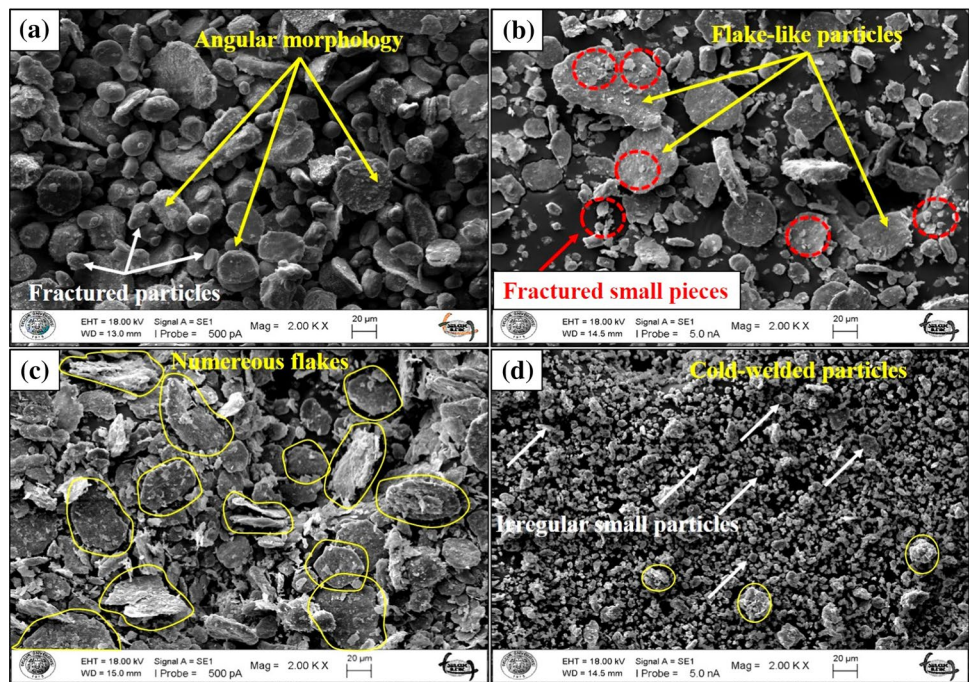


Fig. 2 Schematic representation of ball milling and hot pressing process

Fig. 3 SEM images of CNTs-reinforced Al7075 alloy composite powders with different ball milling times **a** 1, **b** 2, **c** 4, and **d** 8 h

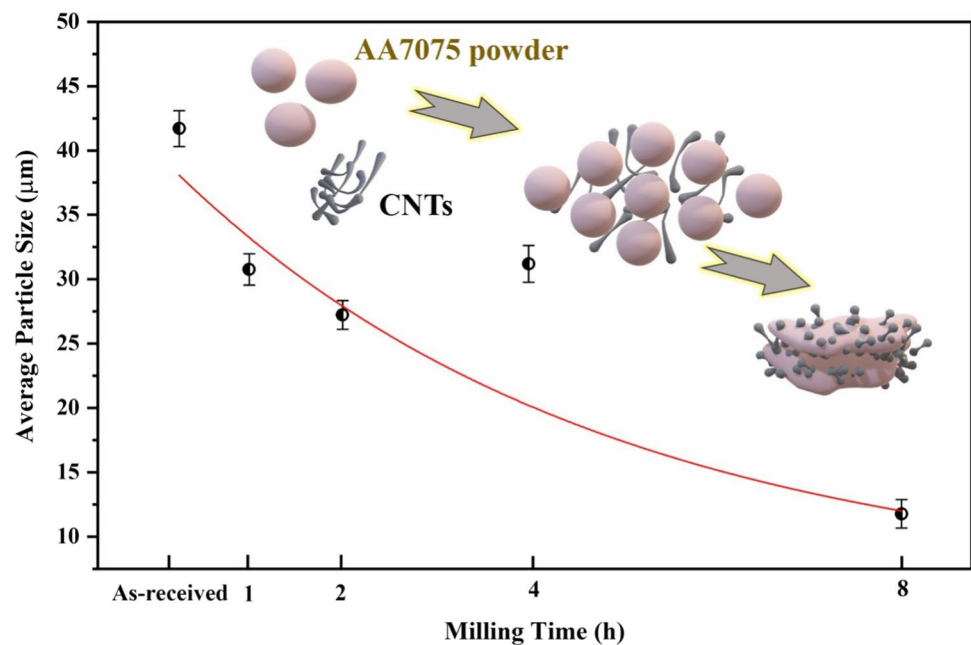


and some of them fractured into tiny pieces without any cold welding (See Fig. 3a). After milling for 2 h, the APS decreased to ~27 μm (See Fig. 4) under the shearing effects of balls, and they exhibited flake-like and fractured irregular particle morphology. When ball milling time was 4 h, although a decrement in particle size was expected because of the fragmented particles, the APS was increased ~31 μm

(Fig. 4) due to numerous flake-like particles, as shown in Fig. 3c.

Further milling for 8 h resulted in a severe decrease of the APS to ~11 μm (See Fig. 4), and many mixture powders were fragmented and showed irregular morphologies, as seen in Fig. 3d. This observed phenomenon originated from a cold working mechanism induced by a long-duration

**Fig. 4** The variation of average particle size as a function of ball milling time



shearing effect, leading to decreased ductility and resultant fragmentation of particles. The dispersed reinforcements (CNTs), on the other hand, concomitantly underwent a significant reduction in particle size. The variation in particle morphology to flake-like pieces (flattened particles) after 1, 2, and especially 4 h of milling was attributed to the repetitive flattening under the impact of the tiny and rigid tungsten carbide (WC) balls. In other words, the observed flattened particle morphology was due to the severe ball–powder–jar and ball–powder–ball collisions during the high-energy planetary ball milling process. Similar observations regarding flake-like morphology in the early stages of milling were reported by some studies [42, 43] when ball milling of the CNT–Al system. However, the milled powders experienced a morphology vary from flattened structure to irregular structure with prolonging milling time since a dynamic balance between fracture and agglomeration mechanisms was achieved at the last phases of milling.

The particle size distribution (PSD) of the mixture powders as a function of milling time is shown in Fig. 5. One observes that the PSD of as-received Al7075 powder was monomodal and narrow, which means that the PSD curve has only one maximum peak. Plus, the particle morphology was almost entirely equiaxial as compared to 1, 2, and 4 h milled powders, as can be confirmed by inspecting Figs. 3a–c. At the same time, an extensive PSD was observed in powders that were milled for 8 h, with the distribution broadening as the milling time was prolonged from 1 to 8 h. Furthermore, the PSD tended to asymmetric behavior with increasing milling time up to 4 h, as seen in inset of Fig. 5. This behavior was ascribed to the plastic deformation and flattening of the powders due to extreme milling

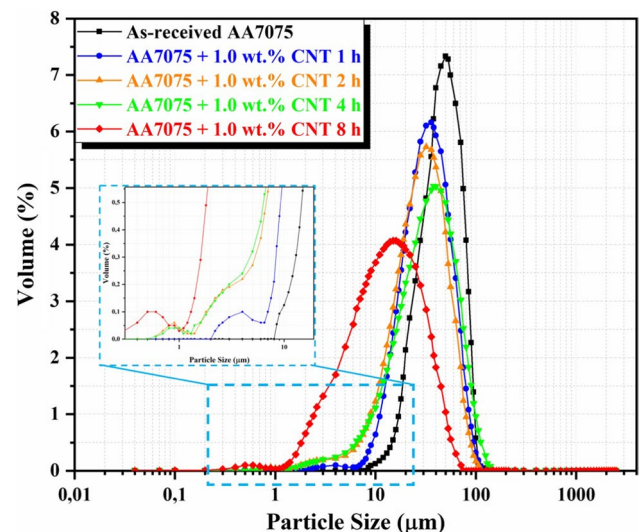


**Fig. 5** The changes of particle size distribution by volume with different milling times

circumstances caused by WC ball collisions, which also appeared to mask variations in the PSD of CNTs. As shown in both Fig. 3d and Fig. 5, the trend mentioned above in morphology and PSD entirely changed when milling time was increased to 8 h. The PSD exhibited clear deflection toward the smaller particles' region due to the dominant fracture mechanism at the final stage of milling. In other words, there was a transformation from flake-like particle morphology to a fine equiaxed particle morphology (see Figs. 3c, d). Therefore, the monitored particle size of these milled powders, their distribution, and morphology, which were milled



for 8 h, were attained due to severe work hardening of the Al7075 matrix, resulting in fracture into small particles.

To investigate the dispersion behavior of CNTs more precisely within the Al7075 matrix, detailed SEM–EDS observations of surfaces of the milled powders were performed, as shown in Fig. 6. For mapping observations, the copper tape was used instead of carbon tape to evaluate the CNT distribution more accurately. It was obviously seen that the dispersion uniformity of CNTs was gradually developed as the milling time increased. Considering the initial milling stage (1 h), the entangled CNT agglomerations were detected on the matrix powder surface (Fig. 6a). When prolonging milling time to 2 h, the amount of these agglomerations decreased (Fig. 6b). Further milling time (4–8 h) resulted in nearly no CNT agglomerations on the surfaces, and many of them were dispersed on the surface and edges of the matrix powders Figs. 6c, d. As the milling time increased, CNTs were shortened, and CNT agglomerations were fractured and redispersed by effective shearing force. Plus, CNTs were gradually embedded into the Al7075 matrix by severe plastic

deformation of the matrix under the tiny and rigid WC balls and a highly influential process control agent in the early milling phase.

Figure 7a shows the XRD curves of the as-received Al7075 and mixture powders as a function of milling time. The observed five primary reflections appertain to the face-centered cubic (fcc) structure of Al matrix ((JCPDS card No. #98-006-4700), while no discernible reflections for CNTs were observed. The absence of CNTs reflections and matching, no intermetallic phases were related to their small proportion of reinforcements and resolution limitation of the X-ray to identify peaks with below 1 wt.%. The dispersion uniformity of CNTs within the Al7075 matrix, undesirable strain circumstance, and amorphization of CNTs could also be other factors for these peaks' absence. According to the X-ray powder diffractograms, the reflections' peak intensity was weakened and broadened as the milling time increased except for 4 h of the milling process. This situation was attributed to a decrement in crystallite size, resulting from the development of structural defects originating from

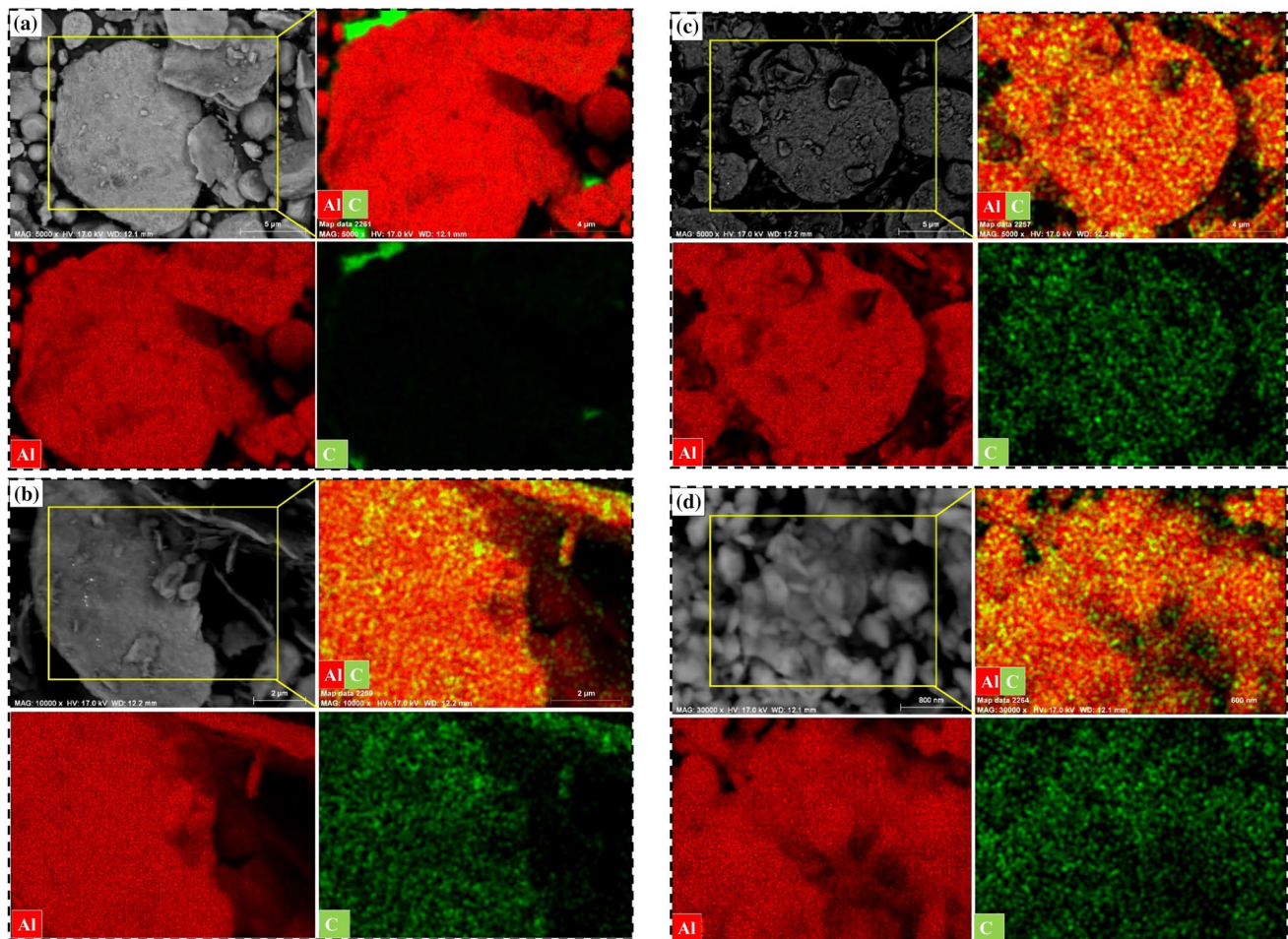


**Fig. 6** SEM–EDS images of milled powders with respect to different milling times: **a** 1, **b** 2, **c** 4, and **d** 8 h

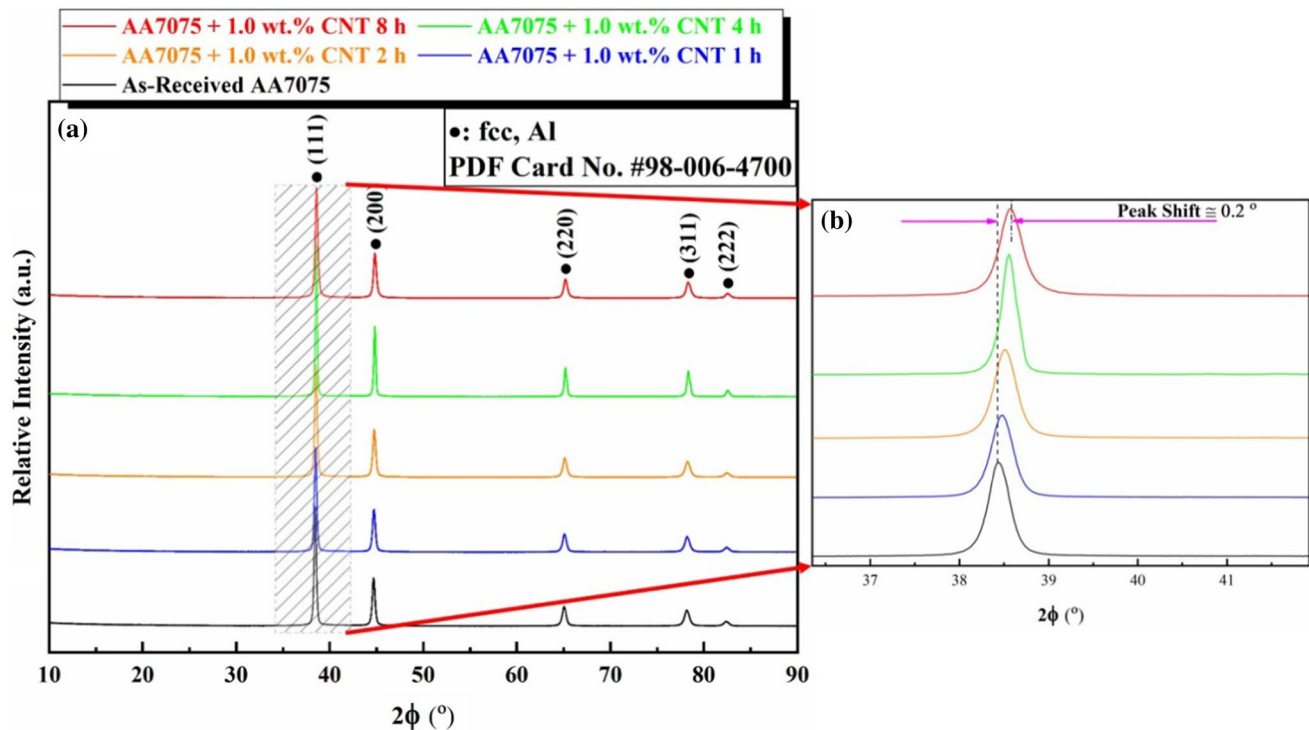


**Fig. 7** **a** XRD patterns of as-received Al7075 and milled powders with different ball milling times, and **b** A closer examination of the (111) Al main reflection showing peak shift

excessive plastic deformation mechanism with increasing milling time. The compositional fluctuations, strain accumulation vicinity of atoms, stacking faults, dislocations, and other structural defects manifesting themselves as micro-strain are also other significant parameters, as they directly or indirectly affect the crystallographic properties reported by Suryanarayana [44]. The XRD curves exhibited peak broadness and the resultant decrease in peak intensities with an increment in ball milling time. When the ball milling time was 4 h, the main peak intensity tended to increase. This was related to an increase in crystallite size (Fig. 8) on the fcc of the Al matrix system and consequent texture formation. As depicted in Fig. 8, while the crystallite size of the as-received powder (unmilled) was measured as 37.21 nm, the crystallite size increased to 41.54 nm when milling time was reached to 4 h. This result complemented the particle morphology image presented in Fig. 3c, where flake-like particles with ~500 nm thickness were observed in mixture powders that were milled for 4 h. The observed texture form was attributed to the plastic deformation incurred by the particles from the high-velocity impact of WC balls during the ball milling process (See Fig. 3c). Different plastic deformation methods such as cold/hot rolling, cold working, work hardening, and ball milling could lead to such effects. A closer examination of the main diffraction patterns of the powders depicted in Fig. 7b showed a noticeable peak shift toward

higher diffraction angles. Such a shift meant that the fcc unit cell volume of the Al matrix decreased with increasing milling time. This situation could have resulted from solid solution, dissolution of CNTs or minor alloying elements in the matrix, and stress accumulation on the lattice, which are triggered by the ball milling system due to the severe plastic deformation under the ball–powder–jar collisions. Therefore, it could be stated that CNTs were appropriately dissolved or embedded into the Al matrix through increasing milling time. The aforementioned dissolution mechanism, which leads to peak shifts, was restricted at the later milling period due to the homogeneous distribution of CNTs; so, the peak displacement showed lower deviation compared to the earlier stage of milling. Moreover, it is noteworthy that there is no encountered aluminum carbide ( $Al_4C_3$ ) peak in the present milling protocol since it is frequently observed in the CNTs–Al hybrid system produced with liquid or powder metallurgy. The assertion above can be substantiated by the fact that the powders were milled for 20 min, followed by 10 min of resting to ensure no substantial temperature rise had taken place. Hence, no chemical reaction of the matrix and reinforcement elements were expected due to the lack of thermal activation for diffusional processes. Similar observations were also declared by Basariya et al. [45] and Esawi et al. [46] in ball milling studies in Al–CNT systems.



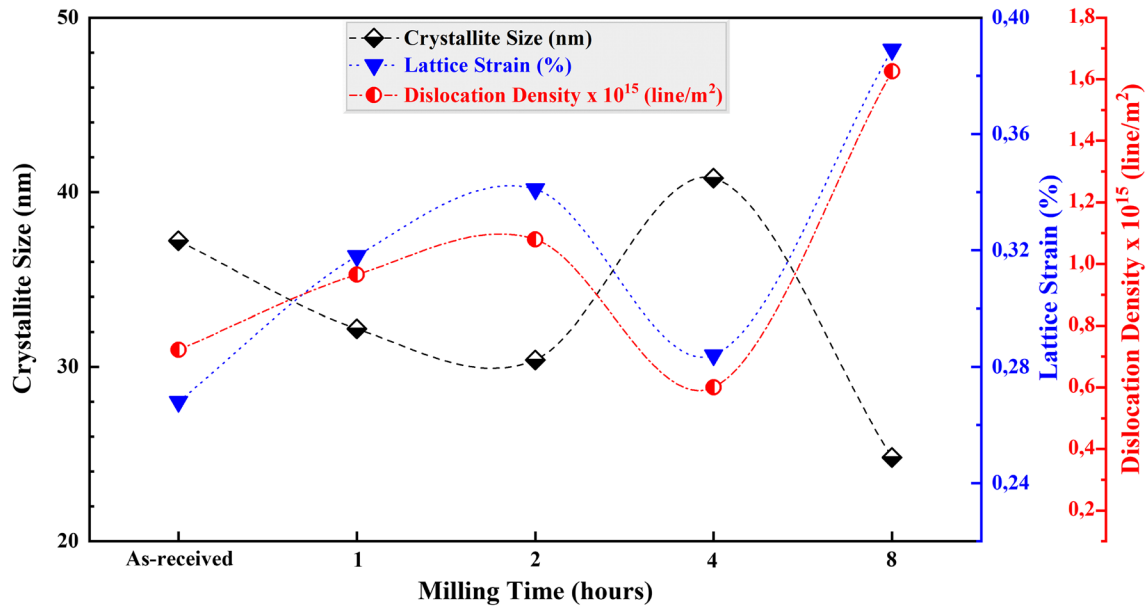


**Fig. 8** The variation of crystallographic properties of milled powders as a function of milling time

Figure 8 shows the crystallographic properties, namely crystallite size, lattice strain, and dislocation density of as-received and milled powders for different milling times. The crystallite size of the as-received Al7075 powder (no milling) was calculated as 37.21 nm, as shown in Fig. 8. At the final milling stage (8 h), the crystallite size decreased to 24.43 nm, which meant that the lattice strain and dislocation density had further increased to  $\sim 0.722$  and  $1.626 \times 10^{15}$  line/m<sup>2</sup>, respectively. The observed decrement in crystallite size was related to increasing dislocation density and stress accumulation in the lattice with excessive plastic deformation due to high-energy ball milling. Besides, uniformly dispersed CNTs in the Al matrix after 8 h of milling hindered dislocation mobility and consequent higher dislocation density. Zare et al. [47] reported that such an increment in dislocation density triggered the formation of sub-boundaries and grain refinement mechanisms. They also declared that uniformly dispersed CNTs in the Al matrix prohibit the easy diffusion paths of mobile dislocations. However, 4 h of milling process could not commit such an effect on the crystallographic properties. As depicted in Fig. 8, the continuous decrease in crystallite size corresponding to increasing lattice strain and dislocation density was interrupted at 4 h of milling. Such characteristic was attributed to numerous flake-like particles, which resulted in texture formation on the fcc structure of the Al matrix. These outcomes were also in harmony with the visible increase in intensity and sharpness of the main reflections of the 4 h milled powders' XRD spectra. As reported by Mokdad et al. [48], flakes and resultant texture formation in the fcc crystal structure of Al matrix was initiated by the deformation process, which is

herein particularly dominant plastic deformation resulting from micro-rolling effects under the rigid WC balls.

To evaluate the destruction of the CNTs for different milling duration, Raman spectroscopic analysis was also performed. In the Raman spectroscopy results given in Fig. 9 for different milling times, it was observed that the graphitic (G) band peak intensity was lower than the defect (D) band peak intensity. Evaluating this observation together with the findings in SEM and TEM images, as shown in Fig. 6 and Fig. 15, respectively, it was re-confirmed that CNTs used in the present study were MWCNTs. In the Raman spectrums, the D and G bands showed the characteristics of the CNTs

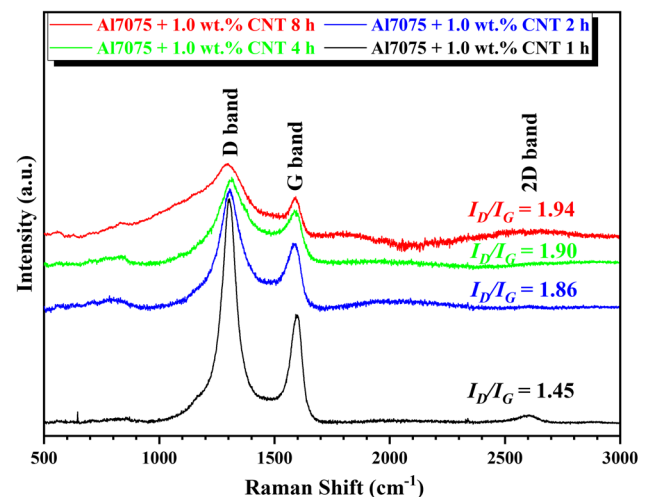


**Fig. 9** Raman spectrums of CNT/Al powders as a function of ball milling time

structure, and they typically located around at  $1350\text{ cm}^{-1}$  and  $1580\text{ cm}^{-1}$ , respectively. In general, the D band shows the existence of defects in the CNTs, and the G band shows crystalline carbon structures [49]. In other words, the intensity of the G band indicates that the structure has  $sp^2$  hybridization, and the D band indicates the presence of defects (locating atoms, dislocations, residual stresses, etc.) in the structure [50]. As the milling time increased, the relative intensity of these peaks gradually decreased. Hence, the fraction volume of trapped CNTs within the ductile matrix was increased with prolonging milling time due to high collisions of powders and balls. In mechanically activated powders, the intensities of these bands decreased and broadened due to increased structural defects and resultant higher dislocation density stemmed from excessive plastic deformation with increasing milling time. They also gradually showed a deflection toward the right side, indicating a peak shift. Besides, the  $I_G/I_D$  ratio, which is calculated from the area under these peaks, indicates the damage degree or quality of the CNTs. Commercially graded CNTs showed an  $I_D/I_G$  ratio of  $\sim 1.11$ , which was adequate for various industrial applications [43]. However, this study's outcomes showed that the  $I_D/I_G$  ratio increased with extended ball milling time. This behavior was attributed that the structure quality of CNTs underwent severe damage with increasing milling time. According to  $I_D/I_G$  ratios shown in Fig. 9, there was no substantial difference in the  $I_D/I_G$  ratio of CNTs after 2 h of milling, revealing no discernible damage on the CNTs. However, at the earlier milling stage (1 h), the  $I_D/I_G$  value increased to 1.45, showing significant damage to CNTs structures. As the milling time extended, although the CNTs were more homogeneously distributed in the matrix, the destruction of the CNTs became more severe regarding Raman results. Hence, to achieve good structural integrity or higher packing density, the ball milling process should control in a precise manner with appropriate time intervals to obtain homogenous dispersion of the CNTs with minimal damage degree.

### 3.2 Effect of milling time on properties of sintered composites

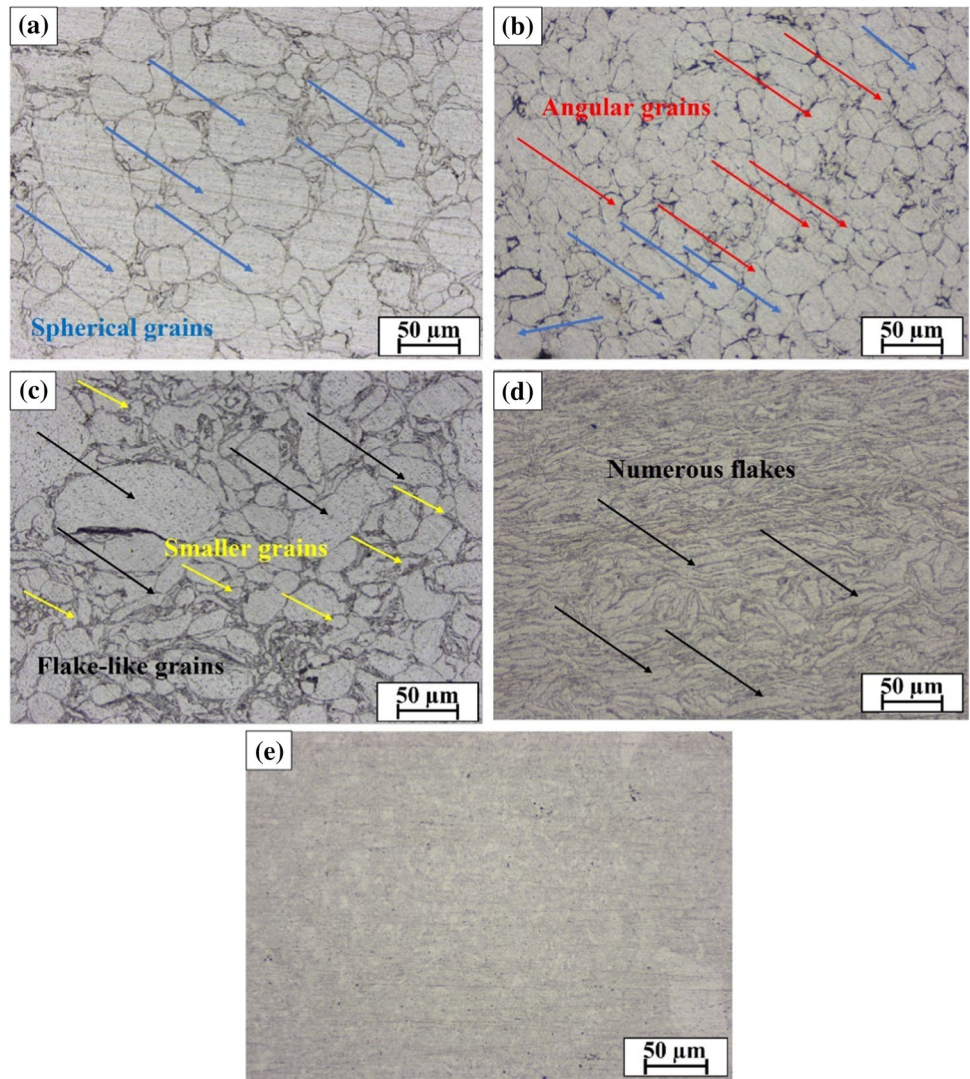
Particle characteristic (e.g., particle size and their distributions and morphologies) is a very crucial point since it significantly affects the sintered composites' microstructure and accompanying structural integrity. In this context, to enhance powders' sintering and packing ability, control and optimization of their characteristics should be addressed carefully. Figure 10 shows the optical microstructure (OM) images of unetched pure Al7075 and Al7075-CNT composites at different ball milling times. Bulk Al7075 alloy, which is produced with as-received Al7075 powder, exhibited spherical grains with a mean size of  $40\text{ }\mu\text{m}$ , as shown in

Fig. 10a. After 1 h of milling, some of these grains turned into angular grains, while many of them remained spherical with lesser grain size, as seen in Fig. 10b. The average grain size of the 1 h milled powders was measured as  $\sim 31\text{ }\mu\text{m}$ . As the milling time increased up to 4 h (Figs. 10c, d), the grain shape of the particles changed to flake-like morphologies. Such morphologies resulted in an increment in grain size, as shown in Fig. 10d. The mean size of the grains increased to  $\sim 34\text{ }\mu\text{m}$  after milling for 4 h due to the formation of flake-like particles as discussed before (as seen in Fig. 4). Further milling for 8 h resulted in randomly fractured grain morphology and concomitantly a considerable reduction in grain size to  $\sim 12\text{ }\mu\text{m}$  due to the repetitive severe collisions of the powders, as seen in Fig. 4 and Fig. 10e. As the milling time increased, the grain size gradually decreased, which shows good agreement with the SEM images and particle size analyses of milled powders. Considering reported some studies regarding the nanostructure formation during the ball milling process [26, 51], it was reported that shear bands were occurred in the early stage of ball milling due to excessive plastic deformation mechanism under the high-energy impact of balls. Figure 11 illustrates the schematic picture of the nano-sized grain formation mechanism induced by the ball milling process.

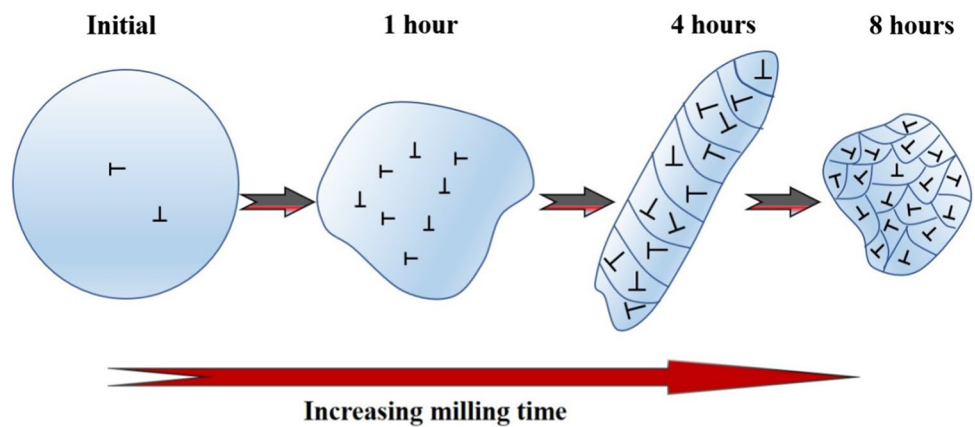
Porosity, which is reversely correlated with the packing ability of the powders, is an unavoidable outcome of the consolidated products fabricated by powder metallurgy (PM) routes [52, 53]. For this reason, SEM observation of the etched bulk composite produced by 8 h milled powders was carried out to understand variations in structural characteristics and pores dependent on the milling time, as seen in Fig. 12. As mentioned in OM images, the sintered samples' grain size was decreased with increasing milling time, and uniform dispersion of CNTs in the matrix was achieved. However, when milling time was extended up to 8 h, it was observed that many micro voids and pores in the structure, as depicted in Fig. 12. This resulted in poor interfacial bonding quality and structural integrity. The effects of such microstructural changes on the relative densities of sintered samples will be discussed in the following sections.

Figure 13 shows the relative densities of the sintered pure Al7075 and Al7075-CNTs composites for different milling times. The density of sintered parts, especially MMCs produced by PM methods, has been significantly influenced by seven key parameters, namely; production parameters, matrix and reinforcement properties, interfacial bonding, structural integrity, distribution, destruction of reinforcements, sintering ability, and perhaps most significantly packing ability [54]. The sintered specimen consisting of relatively bigger particles cannot show the full density. Although smaller particles are expected to be sintered effortlessly than large ones with the same producing history, they cannot also exhibit full density [2]. To obtain optimum packing density,

**Fig. 10** The OM images of composites produced by **a** as-received Al7075, **b** 1, **c** 2, **d** 4, and **e** 8 h milled powders



**Fig. 11** The grain formation mechanism induced by the different ball milling times



it is required to achieve the demanded particle size ranges and morphologies, as reported by German [55]. Considering relative density results in Fig. 13, it was observed that the specimen produced by 2 h milled powders exhibited the

highest density due to the best packing and sintering ability of these powders comprising both flake-like and small grain formations, which led to better interfacial bonding and resultant rigid structural integrity. As mentioned in SEM



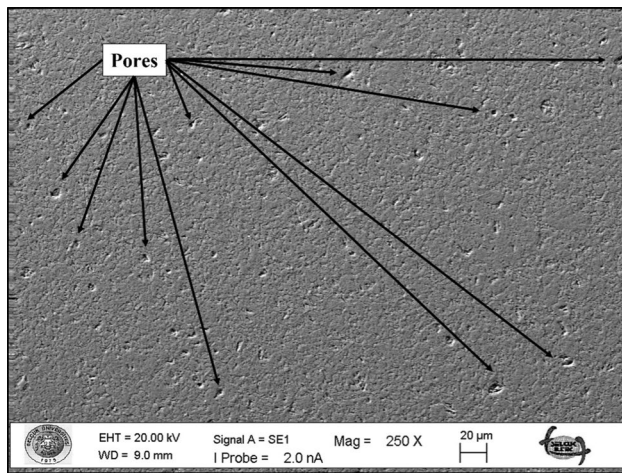


**Fig. 12** SEM image showing micro voids and pores in the 8 h milled sample

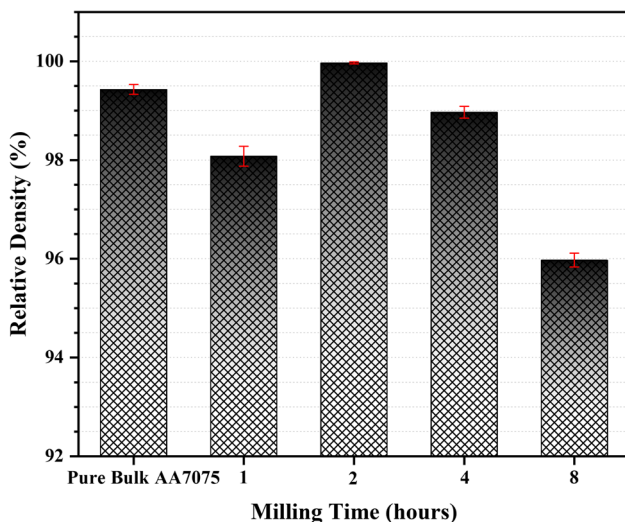


**Fig. 13** The changes of the relative density of pure Al7075 and CNT–Al7075 composites with different ball milling times

results of both milled powders and sintered specimens, the non-uniform dispersion of CNTs and CNT clusters at the initial stages of the milling resulted in more inferior bonding quality between CNTs and Al matrix interface. Such microstructural observations led to an increased plastic strain in the clustered regions, and these regions provided void and pore forms in the material system. Even though the final milling stage (8 h) enhanced the dispersion uniformity of the CNTs within the matrix, severe plastic deformation caused by extending milling time created high hardness in particles and changes in particle size and morphology. Thus, this observed action adversely affected the sintering and packing ability of particles. These outcomes were also consistent with some studies in the literature stating that

prolonging milling time increased hardness but decreased plasticity due to the work hardening mechanism [56]. Work hardening effect, resulting from severe plastic deformation with increasing milling time, triggered numerous nano-sized to micro-sized void formations in the composite produced by 8 h milled powders, as indicated in Fig. 10e. Dolata-Grosz et al. [57] and Zebarjad et al. [58] also reported that the pores in structure negatively affected structural integrity due to their stress concentrator's behavior.

The milling time dependence of the Al7075–CNT composites' Brinell hardness is shown in Fig. 14. A ~160% remarkable increase in hardness from 91 to 237 HB was observed for specimen produced by 8 h milled powders, significantly larger than the plastically deformed materials by conventional means. A nonlinear regression to the data in Fig. 14 gives an empirical equation for the hardness–milling time relation with an  $R^2$  of 99.8%. The origin of the achieved enhancement in hardness could be related to several simultaneous parameters: (i) increased lattice strain, resulting from excessive plastic deformation during milling, and increased dislocation density in particles; (ii) solid solution hardening originating from the dissolution of CNTs and a minor alloying element in the Al matrix; (iii) the decrease in particle size of the 8 h milled powder was small, i.e., ~11  $\mu\text{m}$ , and it can be calculated based on Hall–Petch equation, and thus the probability of finding ways (voids and vacancies) is lower than that for larger particles; (iv) the uniformly dispersed CNTs with nanoscale dimensions in the Al matrix interrupts dislocation mobility and provides strain hardening [59], which can be explained by the Orowan mechanism within the framework dispersion strengthening; (v) increase in the particles' hardness and brittleness due to dominant plastic deformation with prolonging milling procedure; (vi) thermal mismatch mechanism between reinforcement (CNTs) and matrix (Al7075) due to significant differences in coefficient of thermal expansion of CNTs and Al7075, which consequently resulted in work hardening effect. However, the last parameter (vi) effect was negligible in this experiment due to the milled and rested milling protocol, which hinders rising temperature during milling. In conclusion, achieving a significant increase in hardness was a combined influence of the different strengthening mechanisms discussed in (i–vi). However, mechanisms (i–iv) were speculated to be the dominant ones according to previous analyses.

To further verify the hypothesis regarding strengthening mechanisms (iii–iv), the elemental dispersion of reinforcement (CNTs) and matrix (Al) was conducted employing energy-dispersive spectroscopy (EDS) in the mapping mode with high-resolution transmission electron microscopy (HR-TEM). As figured out in Fig. 15, the EDS signals from CNTs and Al were superposed on the cross section of the 8 h milled powders surface. The dispersion of CNTs was found to be homogenous throughout the matrix,

**Fig. 14** Brinell hardness of the CNT–Al composites as a function of the milling time

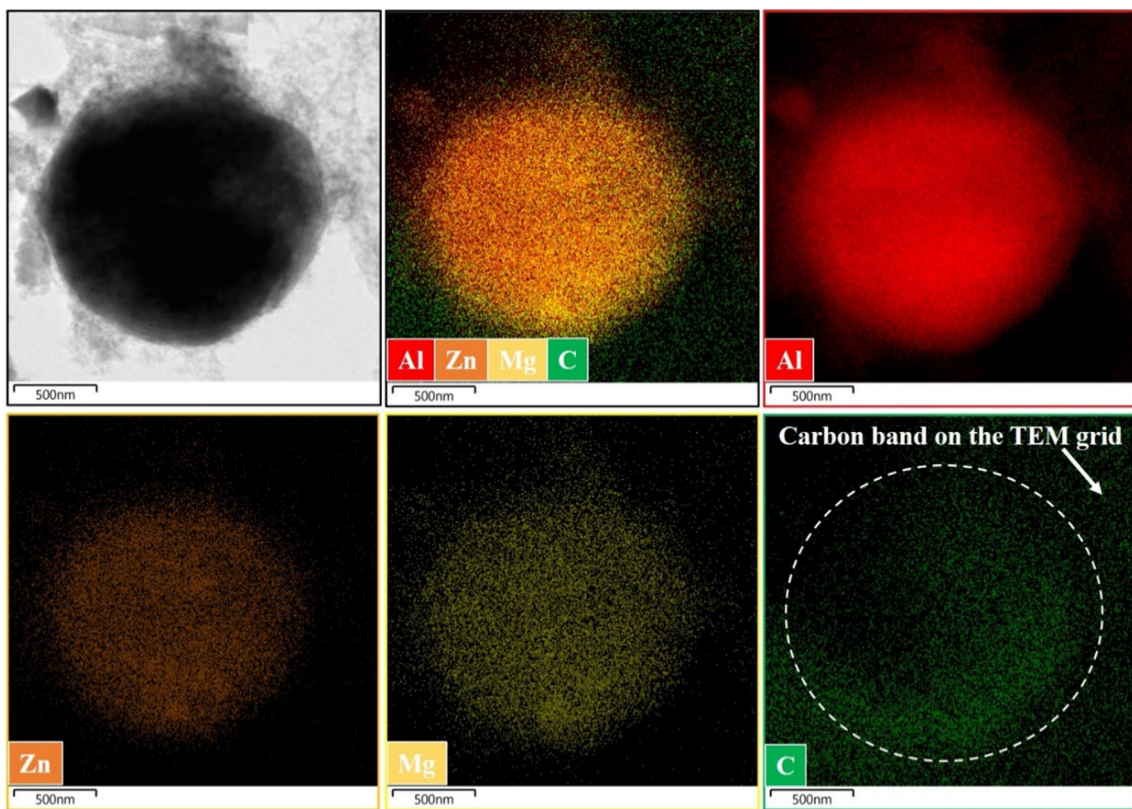
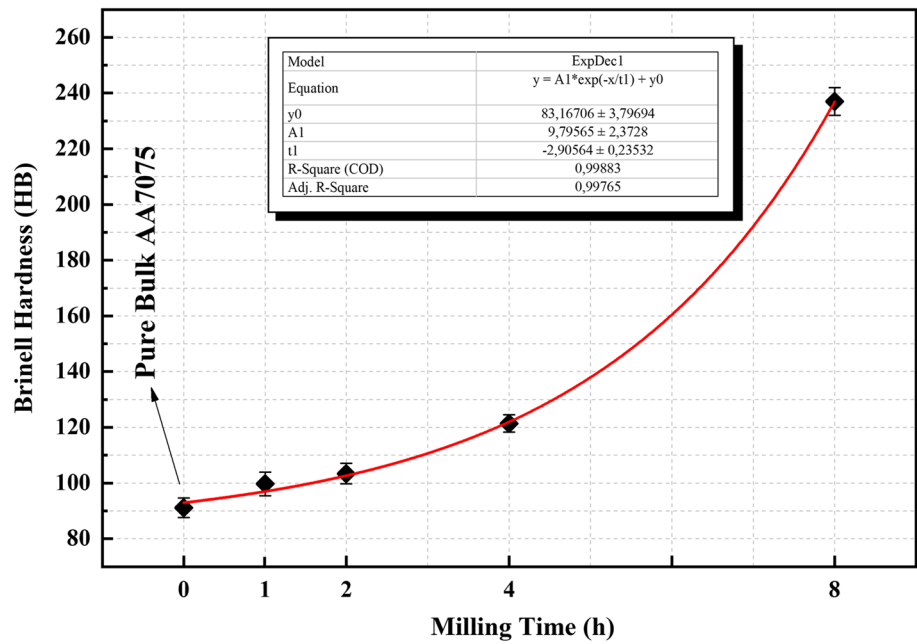
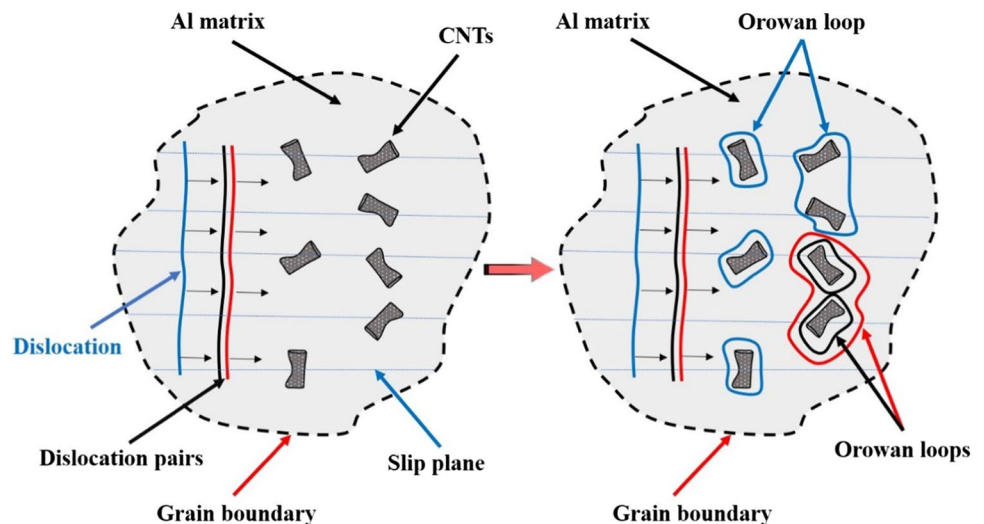


**Fig. 15** HR-TEM-EDS mapping of 8 h milled powders, representing uniform dispersion of the CNTs in the Al matrix

which confirms our hypothesis about the contribution of strengthening mechanisms (iii–iv). Finally, the homogeneously dispersed CNTs would improve the hardening of the matrix by the Orowan looping mechanism. A schematic

illustration of the Orowan looping mechanism is illustrated in Fig. 16. When gliding dislocation or dislocation pairs throughout the matrix’s slip plane interacted or bypassed with CNTs, they began to bend or left Orowan loop(s)

**Fig. 16** A schematic illustration of the Orowan mechanism showing dislocations loops around the CNTs



around CNTs. A higher force is required to drive more dislocations to bypass the CNTs by leaving more Orowan loops around the CNTs, resulting in an enhancement in the hardness of the composites. Different researchers observed similar Orowan loops surrounding the CNTs in the Al matrix system. [60]. This observation, in turn, was also in conformity to the Raman results of Fig. 9. Furthermore, the inter-particle spacing among CNTs was monitored to be uniform and on the order of the nanoparticle size itself. Such short-ranged dispersions of CNTs hindered dislocation movements, causing a higher dislocation density throughout even one minor particle, and concomitant strain hardening because of the Orowan mechanism was also observed by Yoo et al. [61] and Hassanzadeh-Aghdam et al. [62] in the CNT–Al systems. As reported by George et al. [63], increasing dislocation density also triggered the grain refinement mechanism and supplied many refined sub-grains into the matrix. The diverse arrangement of adjacent sub-grains and a large amount of lattice distortion locality at the grain boundaries prevented dislocation movement in the certain slip plane, resulting in an increment in the hardness. Other complementary benefits associated with nanoscale dispersion of CNTs, such as sub-grain formation leading to dislocation pinning, were also reported [64]. What was observed in the present study by using analytical methods such as Raman, XRD, SEM, HR-TEM, and EDS agrees with the phenomena reported in the literature. However, the result of this study distinguished itself in terms of the ~160% increase in hardness. This achieved hardness value was profoundly higher than ball-milled CNTs-reinforced Al matrix composite systems reported by various researchers [65–73]. Such a remarkable hardness increment was attributed to the combined effect of different strengthening mechanisms currently in the CNT–Al7075 composite milled for 8 h.

## 4 Conclusions

The effects of ball milling time on the dispersion behavior of CNTs within the Al7075 matrix system were investigated within the framework of strengthening mechanisms and via ball milling. The influence of ball milling time on the structural and crystallographic properties of mixing powders and their impacts on the microstructural evolution, hardness, and relative density of produced CNT–Al7075 composites was thoroughly characterized by particle size analysis, particle size distribution, SEM, XRD, HR-TEM, optic microscopy analyses, and hardness and density measurements. The following main results and the conclusive remarks could be drawn from the present study.

- As the ball milling time increased, the mean particle size of mixture powders decreased. Raman spectrum, SEM, and HR-TEM observations showed that the CNTs were shortened to a large extent and uniformly distributed and embedded into the ductile Al7075 matrix. Also, TEM–EDS mapping mode demonstrated that 8 h of milling ensured the homogeneous dispersion of CNTs as nanoscopic dimensions.
- The Orowan mechanism was assumed to be the dominant hardening mechanism in the CNTs–Al7075 hybrid system. A remarkable increment in Brinell hardness from 91 to 237 HB (~160%) was achieved in the composite produced by 8 h milled powders. The observed ~160% increase in hardness was ascribed to the high population of uniformly distributed nanoscopic CNTs interior or exterior regions of the powder particles, reduced particle size, increasing lattice strain, and dislocation density.
- The combined effects of work hardening, dispersion uniformity of CNTs, and increased hardness of powders improve the samples' hardness. However, packing



and sintering performance and resultant density values were adversely affected by these circumstances due to increased deformation hardening by further milling process. Hence, a porous structure occurs, which has a detrimental effect on density.

- Based on the above discourse, the present study's outcomes revealed that the production history of mixture powders had a critical effect on the end of CNT–Al product characteristics and performance, which still remain a blind spot in the current literature.

**Funding** This study was not funded.

## Declarations

**Conflict of interest** The authors declare that they have no competing interests.

**Ethical approval** The authors state that the research was conducted according to ethical standards.

**Open Access** This article is licensed under a Creative Commons Attribution 4.0 International License, which permits use, sharing, adaptation, distribution and reproduction in any medium or format, as long as you give appropriate credit to the original author(s) and the source, provide a link to the Creative Commons licence, and indicate if changes were made. The images or other third party material in this article are included in the article's Creative Commons licence, unless indicated otherwise in a credit line to the material. If material is not included in the article's Creative Commons licence and your intended use is not permitted by statutory regulation or exceeds the permitted use, you will need to obtain permission directly from the copyright holder. To view a copy of this licence, visit <http://creativecommons.org/licenses/by/4.0/>.

## References

1. Salur E, Aslan A, Kuntoglu M, Gunes A, Sahin OS. Experimental study and analysis of machinability characteristics of metal matrix composites during drilling. *Compos B*. 2019;166:401–13.
2. Salur E, Acarer M, Şavklıyıldız İ. Improving mechanical properties of nano-sized TiC particle reinforced AA7075 Al alloy composites produced by ball milling and hot pressing. *Mater Today Commun*. 2021;27:102202.
3. Imran M, Khan AA. Characterization of Al-7075 metal matrix composites: a review. *J Mater Res Technol*. 2019;8:3347–56.
4. Jiang L, Li Z, Fan G, Cao L, Zhang D. The use of flake powder metallurgy to produce carbon nanotube (CNT)/aluminum composites with a homogenous CNT distribution. *Carbon*. 2012;50:1993–8.
5. Aslan A, Salur E, Düzcükoğlu H, Şahin ÖS, Ekrem M. The effects of harsh aging environments on the properties of neat and MWCNT reinforced epoxy resins. *Constr Build Mater*. 2021;272:121929.
6. Chen M, Fan G, Tan Z, Yuan C, Xiong D, Guo Q, Su Y, Naito M, Li Z. Tailoring and characterization of carbon nanotube dispersity in CNT/6061Al composites. *Mater Sci Eng A*. 2019;757:172–81.
7. Guo B, Ni S, Yi J, Shen R, Tang Z, Du Y, Song M. Microstructures and mechanical properties of carbon nanotubes reinforced pure aluminum composites synthesized by spark plasma sintering and hot rolling. *Mater Sci Eng A*. 2017;698:282–8.
8. Güneş A, Şahin ÖS, Düzcükoğlu H, Salur E, Aslan A, Kuntoğlu M, Giasin K, Pimenov DY. Optimization study on surface roughness and tribological behavior of recycled cast iron reinforced bronze MMCs produced by hot pressing. *Materials*. 2021;14:3364.
9. Jargalsaikhan B, Bor A, Lee J, Choi H. Al/CNT nanocomposite fabrication on the different property of raw material using a planetary ball mill. *Adv Powder Technol*. 2020;31:1957–62.
10. Dhore VG, Rathod W, Patil K. Investigation of mechanical properties of carbon nanotubes reinforced aluminium composite by metal injection molding. *Mater Today Proc*. 2018;5:20690–8.
11. Li Q, Rottmair CA, Singer RF. CNT reinforced light metal composites produced by melt stirring and by high pressure die casting. *Compos Sci Technol*. 2010;70:2242–7.
12. Yang X, Zou T, Shi C, Liu E, He C, Zhao N. Effect of carbon nanotube (CNT) content on the properties of in-situ synthesis CNT reinforced Al composites. *Mater Sci Eng A*. 2016;660:11–8.
13. Laha T, Chen Y, Lahiri D, Agarwal A. Tensile properties of carbon nanotube reinforced aluminum nanocomposite fabricated by plasma spray forming. *Compos A*. 2009;40:589–94.
14. Mohammed SM, Chen DL. Carbon nanotube-reinforced aluminum matrix composites. *Adv Eng Mater*. 2020;22:1901176.
15. Fan G, Jiang Y, Tan Z, Guo Q, Xiong D-B, Su Y, Lin R, Hu L, Li Z, Zhang D. Enhanced interfacial bonding and mechanical properties in CNT/Al composites fabricated by flake powder metallurgy. *Carbon*. 2018;130:333–9.
16. Salur E, Nazik C, Acarer M, Şavklıyıldız İ, Akdoğan EK. Ultra-high hardness in Y2O3 dispersed ferrous multicomponent nanocomposites. *Mater Today Commun*. 2021;28:102637.
17. Abbas A, Huang SJ, Balloková B, Sülleiová K. Tribological effects of carbon nanotubes on magnesium alloy AZ31 and analyzing aging effects on CNTs/AZ31 composites fabricated by stir casting process. *Tribol Int*. 2020;142:105982.
18. Li M, Chen M, Wu Z, Liu J. Carbon nanotube grafted with polyalcohol and its influence on the thermal conductivity of phase change material. *Energy Convers Manage*. 2014;83:325–9.
19. Deyab M. Corrosion protection of aluminum bipolar plates with polyaniline coating containing carbon nanotubes in acidic medium inside the polymer electrolyte membrane fuel cell. *J Power Sources*. 2014;268:50–5.
20. Yang J, Xiao S, Yuyong C, Xu L, Wang X, Zhang D, Li M. Effects of nano-Y2O3 addition on the microstructure evolution and tensile properties of a near- $\alpha$  titanium alloy. *Mater Sci Eng A*. 2019;761:137977.
21. Kwon H, Park DH, Silvain JF, Kawasaki A. Investigation of carbon nanotube reinforced aluminum matrix composite materials. *Compos Sci Technol*. 2010;70:546–50.
22. Jagannatham M, Chandran P, Sankaran S, Haridoss P, Nayan N, Bakshi SR. Tensile properties of carbon nanotubes reinforced aluminum matrix composites: a review. *Carbon*. 2020;160:14–44.
23. Nazik C, Tarakcioglu N, Ozkaya S, Erdemir F, Canakci A. Determination of effect of B 4 C content on density and tensile strength of AA7075/B 4 C composite produced via powder technology. *Int J Mater Mech*. 2016;4:251–61.
24. Casati R, Fiocchi J, Fabrizi A, Lecis N, Bonollo F, Vedani M. Effect of ball milling on the ageing response of Al2618 composites reinforced with SiC and oxide nanoparticles. *J Alloys Compd*. 2017;693:909–20.
25. Canakci A, Varol T, Ozsahin S. Prediction of effect of volume fraction, compact pressure and milling time on properties

- of Al-Al<sub>2</sub>O<sub>3</sub> MMCs using neural networks. *Met Mater Int.* 2013;19:519–26.
26. Salur E, Aslan A, Kuntoğlu M, Acarer M. Effect of ball milling time on the structural characteristics and mechanical properties of nano-sized Y<sub>2</sub>O<sub>3</sub> particle reinforced aluminum matrix composites produced by powder metallurgy route. *Adv Powder Technol.* 2021;32:3826–44.
  27. Ghasali E, Sangpour P, Jam A, Rajaei H, Shirvanimoghaddam K, Ebadzadeh T. Microwave and spark plasma sintering of carbon nanotube and graphene reinforced aluminum matrix composite. *Arch Civ Mech.* 2018;18:1042–54.
  28. Poirier D, Gauvin R, Drew RA. Structural characterization of a mechanically milled carbon nanotube/aluminum mixture. *Compos A.* 2009;40:1482–9.
  29. Chen B, Li Z, Shen J, Li S, Jia L, Umeda J, Kondoh K, Li J. Mechanical properties and strain hardening behavior of aluminum matrix composites reinforced with few-walled carbon nanotubes. *J Alloys Compd.* 2020;826:154075.
  30. Turan ME. Investigation of mechanical properties of carbonaceous (MWCNT, GNPs and C60) reinforced hot-extruded aluminum matrix composites. *J Alloys Compd.* 2019;788:352–60.
  31. Mohammed S, Chen D, Liu Z, Ni D, Wang Q, Xiao B, Ma Z. Deformation behavior and strengthening mechanisms in a CNT-reinforced bimodal-grained aluminum matrix nanocomposite. *Mater Sci Eng A.* 2021;817:141370.
  32. Kim H, Babu J, Kang C. Fabrication of A356 aluminum alloy matrix composite with CNTs/Al<sub>2</sub>O<sub>3</sub> hybrid reinforcements. *Mater Sci Eng A.* 2013;573:92–9.
  33. Esawi AM, Morsi K, Sayed A, Taher M, Lanka S. Effect of carbon nanotube (CNT) content on the mechanical properties of CNT-reinforced aluminium composites. *Compos Sci Technol.* 2010;70:2237–41.
  34. Li N, Yang C, Li C, Guan H, Fang D, Tao J, Liu Y, Yi J. Carbon nanotubes reinforced aluminum matrix composites with high elongation prepared by flake powder metallurgy. *Diamond Relat Mater.* 2020;107:107907.
  35. Ostovan F, Matori KA, Toozandehjani M, Oskoueian A, Yusoff HM, Yunus R, Ariff AHM, Quah HJ, Lim WF. Effects of CNTs content and milling time on mechanical behavior of MWCNT-reinforced aluminum nanocomposites. *Mater Chem Phys.* 2015;166:160–6.
  36. Deng C, Wang D, Zhang X, Li A. Processing and properties of carbon nanotubes reinforced aluminum composites. *Mater Sci Eng A.* 2007;444:138–45.
  37. Kurita H, Kwon H, Estili M, Kawasaki A. Multi-walled carbon nanotube-aluminum matrix composites prepared by combination of hetero-agglomeration method, spark plasma sintering and hot extrusion. *Mater Trans.* 2011;52:1960–5.
  38. Zak AK, Majid WA, Abrishami ME, Yousefi R. X-ray analysis of ZnO nanoparticles by Williamson-Hall and size-strain plot methods. *Solid State Sci.* 2011;13:251–6.
  39. Williamson G, Smallman R III. Dislocation densities in some annealed and cold-worked metals from measurements on the X-ray debye-scherrer spectrum. *Philos Mag.* 1956;1:34–46.
  40. Velumani S, Narayandass SK, Mangalaraj D. Structural characterization of hot wall deposited cadmium selenide thin films. *Semicond Sci Technol.* 1998;13:1016.
  41. D.A. Long, Raman spectroscopy, New York, 1 (1977).
  42. Wang L, Choi H, Myoung J-M, Lee W. Mechanical alloying of multi-walled carbon nanotubes and aluminium powders for the preparation of carbon/metal composites. *Carbon.* 2009;47:3427–33.
  43. Xu R, Tan Z, Xiong D, Fan G, Guo Q, Zhang J, Su Y, Li Z, Zhang D. Balanced strength and ductility in CNT/Al composites achieved by flake powder metallurgy via shift-speed ball milling. *Compos A.* 2017;96:57–66.
  44. Suryanarayana C. Mechanical alloying and milling. *Prog Mater Sci.* 2001;46:1–184.
  45. Basariya MR, Srivastava V, Mukhopadhyay N. Microstructural characteristics and mechanical properties of carbon nanotube reinforced aluminum alloy composites produced by ball milling. *Mater Des.* 2014;64:542–9.
  46. Esawi AM, Morsi K, Sayed A, Gawad AA, Borah P. Fabrication and properties of dispersed carbon nanotube–aluminum composites. *Mater Sci Eng A.* 2009;508:167–73.
  47. Zare H, Jahedi M, Toroghinejad MR, Meratian M, Knezevic M. Compressive, shear, and fracture behavior of CNT reinforced Al matrix composites manufactured by severe plastic deformation. *Mater Des.* 2016;106:112–9.
  48. Mokdad F, Chen D, Liu Z, Xiao B, Ni D, Ma Z. Deformation and strengthening mechanisms of a carbon nanotube reinforced aluminum composite. *Carbon.* 2016;104:64–77.
  49. Jagannatham M, Sankaran S, Haridoss P. Microstructure and mechanical behavior of copper coated multiwall carbon nanotubes reinforced aluminum composites. *Mater Sci Eng A.* 2015;638:197–207.
  50. Peng HJ, Huang JQ, Zhao MQ, Zhang Q, Cheng XB, Liu XY, Qian WZ, Wei F. Nanoarchitected graphene/CNT@ porous carbon with extraordinary electrical conductivity and interconnected micro/mesopores for lithium-sulfur batteries. *Adv Funct Mater.* 2014;24:2772–81.
  51. Ezatpour H, Parizi MT, Ebrahimi G. The extraordinary effect of very low content of hybrid carbonaceous reinforcement on the microstructural and mechanical properties of 7075 aluminum alloy. *Arch Civ Mech.* 2021;21:1–24.
  52. Şahin ÖS, Güneş A, Aslan A, Salur E, Karadağ HB, Akdemir A. Low-velocity impact behavior of porous metal matrix composites produced by recycling of bronze and iron chips. *Iran J Sci Technol Trans Mech Eng.* 2019;43:53–60.
  53. Usca ŪA, Uzun M, Kuntoğlu M, Şap S, Giasin K, Pimenov DY. Tribological aspects, optimization and analysis of Cu-B-CrC composites fabricated by powder metallurgy. *Materials.* 2021;14:4217.
  54. Şap S, Uzun M, Usca ŪA, Pimenov DY, Giasin K, Wojciechowski S. Investigation on microstructure, mechanical, and tribological performance of Cu base hybrid composite materials. *J Mater Res Technol.* 2021. <https://doi.org/10.1016/j.jmrt.2021.11.114>.
  55. R.M. German, Particle packing characteristics, (1989).
  56. Ozkaya S, Canakci A. Effect of the B4C content and the milling time on the synthesis, consolidation and mechanical properties of AlCuMg-B4C nanocomposites synthesized by mechanical milling. *Powder Technol.* 2016;297:8–16.
  57. Dolata-Grosz A, Śleziona J, Formanek B. Structure and properties of aluminium cast composites strengthened by dispersion phases. *J Mater Process Technol.* 2006;175:192–7.
  58. Zebarjad SM, Sajjadi S. Microstructure evaluation of Al–Al<sub>2</sub>O<sub>3</sub> composite produced by mechanical alloying method. *Mater Des.* 2006;27:684–8.
  59. Xie K, Zhang G, Huang H, Zhang J, Liu Z, Cai B. Investigation of the main strengthening mechanism of carbon nanotube reinforced aluminum composites. *Mater Sci Eng A.* 2021;804:140780.
  60. Park JG, Keum DH, Lee YH. Strengthening mechanisms in carbon nanotube-reinforced aluminum composites. *Carbon.* 2015;95:690–8.
  61. Yoo S, Han S, Kim W. Strength and strain hardening of aluminum matrix composites with randomly dispersed nanometer-length fragmented carbon nanotubes. *Scripta Mater.* 2013;68:711–4.
  62. Hassanzadeh-Aghdam M, Mahmoodi M. A comprehensive analysis of mechanical characteristics of carbon nanotube-metal matrix nanocomposites. *Mater Sci Eng A.* 2017;701:34–44.

63. George R, Kashyap K, Rahul R, Yamdagni S. Strengthening in carbon nanotube/aluminium (CNT/Al) composites. *Scripta Mater.* 2005;53:1159–63.
64. Chen B, Li S, Imai H, Jia L, Umeda J, Takahashi M, Kondoh K. Carbon nanotube induced microstructural characteristics in powder metallurgy Al matrix composites and their effects on mechanical and conductive properties. *J Alloys Compd.* 2015;651:608–15.
65. Majid M, Majzoobi GH, Noozad GA, Reihani A, Mortazavi SZ, Gorji M. Fabrication and mechanical properties of MWCNTs-reinforced aluminum composites by hot extrusion. *Rare Met.* 2012;31:372–8.
66. Vozniakovskii A, Kidalov S, Kol'tsova T. Development of composite material aluminum-carbon nanotubes with high hardness and controlled thermal conductivity. *J Compos Mater.* 2019;53:2959–65.
67. Raju KSR, Raju VR, Raju PRM, Rajesh S, Partha G. Enhancement of the mechanical properties of an aluminum metal matrix nanocomposite by the hybridization technique. *J Mater Res Technol.* 2016;5:241–9.
68. Tolochko OV, Koltsova TS, Bobrynina EV, Rudskoy AI, Zemtsova EG, Kirichenko SO, Smirnov VM. Conditions for production of composite material based on aluminum and carbon nanofibers and its physic-mechanical properties. *Nanomaterials.* 2019;9:550.
69. Zhou S-M, Zhang X-B, Ding Z-P, Min C-Y, Xu G-L, Zhu W-M. Fabrication and tribological properties of carbon nanotubes reinforced Al composites prepared by pressureless infiltration technique. *Compos A.* 2007;38:301–6.
70. Manjunatha L, Yunus M, Alsoufi MS, Dinesh P. Development and comparative studies of aluminum-based carbon nano tube metal matrix composites using powder metallurgy and stir casting technology. *Int J Eng Res.* 2017;8:521–6.
71. Elshalakany AB, Osman T, Khattab A, Azzam B, Zaki M. Microstructure and mechanical properties of MWCNTs reinforced A356 aluminum alloys cast nanocomposites fabricated by using a combination of rheocasting and squeeze casting techniques. *J Nanomater.* 2014. <https://doi.org/10.1155/2014/386370>.
72. Abbasipour B, Niroumand B, Vaghefi SM. Compcasting of A356-CNT composite. *Trans Nonferrous Met Soc China.* 2010;20:1561–6.
73. Alizadeh A, Abdollahi A, Biukani H. Creep behavior and wear resistance of Al 5083 based hybrid composites reinforced with carbon nanotubes (CNTs) and boron carbide (B4C). *J Alloys Compd.* 2015;650:783–93.

**Publisher's Note** Springer Nature remains neutral with regard to jurisdictional claims in published maps and institutional affiliations.